Received: 7 May 2021 | Revised: 26 August 2021 | Accepted: 7 September 2021

DOI: 10.1096/fj.202100757R

THE FASEB JOURNAL

RESEARCH ARTICLE

Target-specific control of piriform cortical output via distinct inhibitory circuits

He-Hai Jiang[1,2,3] | **Anni Guo**[1,2,3] | **Arthur Chiu**[1,2,3] | **Huanhuan Li**[1,2,3] | **Cora Sau Wan Lai**[4,5] | **Chunyue Geoffrey Lau**[1,2,3]

[1]Department of Neuroscience, City University of Hong Kong, Hong Kong, China

[2]Department of Biomedical Sciences, City University of Hong Kong, Hong Kong, China

[3]Shenzhen Research Institute of City University of Hong Kong, Shenzhen, China

[4]School of Biomedical Sciences, LKS Faculty of Medicine, The University of Hong Kong, Pokfulam, Hong Kong, China

[5]State Key Laboratory of Brain and Cognitive Sciences, The University of Hong Kong, Pokfulam, Hong Kong, China

Correspondence
Chunyue Geoffrey Lau, Department of Neuroscience, City University of Hong Kong, 1B-203, 2/F, Block 1, To Yuen Building, 31 To Yuen Street, Kowloon Tong, Kowloon, Hong Kong, China.
Email: geoff.lau@cityu.edu.hk

Present address
He-Hai Jiang, Bioland Laboratory (Guangzhou Regenerative Medicine and Health-Guangdong Laboratory), Guangzhou, Guangdong, China

Funding information
National Natural Science Foundation of China (NSFC), Grant/Award Number: 31571031; Shenzhen Science and Technology Innovation Commission, Grant/Award Number: JCYJ20190808182203591; FHB | Health and Medical Research Fund (HMRF), Grant/Award Number: 03143096; Research Grants Council, University Grants Committee (RGC, UGC), Grant/Award Number: 27103715, 17128816, 21103818, 11104320 and 11104521

Abstract

Information represented by principal neurons in anterior piriform cortex (APC) is regulated by local, recurrent excitation and inhibition, but the circuit mechanisms remain elusive. Two types of layer 2 (L2) principal neurons, semilunar (SL), and superficial pyramidal (SP) cells, are parallel output channels, and the control of their activity gates the output of APC. Here, we examined the hypothesis that recurrent inhibition differentially regulates SL and SP cells. Patterned optogenetic stimulation revealed that the strength of recurrent inhibition is target- and layer-specific: L1 > L3 for SL cells, but L3 > L1 for SP cells. This target- and layer-specific inhibition was largely attributable to the parvalbumin (PV), but not somatostatin, interneurons. Intriguingly, olfactory experience selectively modulated the PV to SP microcircuit while maintaining the overall target and laminar specificity of inhibition. Together, these results indicate the importance of target-specific inhibitory wiring for odor processing, implicating these mechanisms in gating the output of piriform cortex.

KEYWORDS

GABAergic interneurons, inhibitory connectivity, inhibitory plasticity, sensory experience

Abbreviations: ACSF, artificial cerebrospinal fluid; APC, anterior piriform cortex; CA1, Cornu Ammonis area 1 of the hippocampus; CheTA, channelrhodopsin-2 with fast kinetics; Chrimson, red-shifted channelrhodopsin-2; CNQX, 6-Cyano-7-nitroquinoxaline-2,3-dione; D,L-APV, DL-2-Amino-5-phosphonopentanoic acid; DMD, digital mirror device; E–I ratio, excitation–inhibition ratio; EPSC/IPSC, excitatory/inhibitory postsynaptic current; L1/L2/L3, layer 1/2/3 of the cortex; LED, light-emitting diode; LFP, local field potential; NO, naris occlusion; OB, olfactory bulb; PV, parvalbumin; sIPSCs, spontaneous inhibitory postsynaptic currents; SL, semilunar (neuron); SP, superficial pyramidal (neuron); SST, somatostatin.

1 | INTRODUCTION

For all sensory systems, a key function is to have faithful representation of the stimulus while maintaining the flexibility of adding associative information to it. The anterior piriform cortex (APC) is a primary sensory cortex one synapse downstream of the olfactory bulb (OB), and yet exhibits properties that resemble both a sensory and association cortex.[1] A key feature of the APC is the clear anatomical segregation of the direct, OB input in layer 1a (L1a), from the recurrent (associative) input in L1b. The recurrent pathway in APC is important for a variety of functions including odor concentration-invariant coding[2,3] and mixture demixing.[4] Recurrent excitatory inputs exhibit robust long-term synaptic plasticity,[5–7] which could be important for context-dependent retrieval and storage of memory.[6,8–12] Hence, neurons in APC can extract relevant information about odors depending on context, but how local circuits achieve this is largely unknown.

How is the output of APC gated to represent different odorant features? Our group and others have shown that excitatory principal neurons within L2 form two distinct circuits for routing information out of the APC.[13–17] Specifically, we found that semilunar (SL) cells in L2a and superficial pyramidal (SP) cells in L2b exhibit distinct projection patterns in that SP, but not SL, cells project back to the OB.[17] Since the APC send extensive projections to OB to modulate neural representation and learning,[18,19] regulation of SL and SP neuronal output will significantly impact activity in APC as well as OB. Single principal neurons can extend axons over millimeters in the rostral or caudal direction, forming the recurrent excitatory pathway.[20] These long-range fibers in turn drives local, recurrent inhibition in APC.[6] Recurrent inhibition is the dominant type of inhibition in APC,[21] and is largely mediated by interneurons in the deep layers (L2 and L3), namely the parvalbumin-(PV) and somatostatin (SST)-expressing interneurons. However, how recurrent inhibition and interneuron subtypes control APC output by modulating principal neurons is largely unknown.

Here, we hypothesize that inhibitory circuits differentially control SL and SP cell function in a laminar- and target-specific manner. As neural activity in APC is mostly driven by spiking in the ipsilateral OB,[22] unilateral activity deprivation can illuminate the role of experience in regulating inhibitory circuits in APC. Using sensory experience deprivation, electrophysiology, optogenetics, patterned illumination, and immunofluorescent staining, we examined spontaneous inhibitory postsynaptic currents (sIPSCs), evoked excitatory postsynaptic currents (EPSCs)-IPSCs, and dissected PV and SST interneuronal output. Here, we reveal differential wiring of recurrent inhibition for SL versus SP cells. Moreover, these inhibitory circuits were differentially sensitive to manipulation of upstream neural activity, suggesting the critical yet different roles of SL and SP cells in activity-dependent remodeling of APC circuits.

2 | METHODS AND MATERIALS

2.1 | Animals and genetics

Both male and female mice of *Pvalb-IRES-Cre* mouse line (Jackson Laboratory 008069; referred to as PV-Cre in this manuscript),[23] SST-IRES-Cre (Jackson Laboratory 013044; herein referred to as SST-Cre), and wide-type C57BL/6J were used in this study. All work was done in accordance with guidelines from the Animal Research Ethics Sub-Committees of City University of Hong Kong and Department of Health of Hong Kong SAR government. Naris occlusion (NO) was performed by using an electrocauterizer (WPI) on young adult mice (postnatal day 42–45) with anesthesia 8–10 days before experiment. The closed nostril was checked for its complete closure by visual inspection or application of a drop of detergent on it. After confirmation of occlusion of 8–10 days, mice were used for electrophysiology or microscopy.

2.2 | Stereotaxic injections

To infect local APC neurons (both excitatory and inhibitory), AAV9-Syn-ChrimsonR-tdT (300 nl; Addgene) was stereotaxically injected into both hemispheres of APC (Stoelting) in wide-type C57BL/6J (Nanoject III Programmable Nanoliter Injector, Drummond Scientific Company; 3 to 4 weeks old). To specifically activate interneuron subpopulations, ChETA was expressed in PV cells or SST cells by injecting AAV9-EF1α-DIO-ChETA-EYFP (300–400 nl; Penn Vector Core or Addgene) into both hemispheres of APC in either PV-cre or SST-cre mice. Glass pipettes (1.5 μl, Drummond Wiretrol) were prepared by Narishige PC-10 Puller (Narishige Company) and had tip diameter of ~8–10 μm. The coordinates of APC relative to bregma were: lateral +2.7 mm, anterior +1.5 mm, ventral −3.5 mm. Animals were allowed to recover for 3–4 weeks, then acute APC slices were prepared for electrophysiology or brains were fixed for microscopy. For activity deprivation experiments, 3 weeks after injection, mice were subjected to naris occlusion for 8–10 days (Section 2.1).

2.3 | Brain slice preparation

All experiments used acute brain slices prepared from the APC of wild-type C57BL6/J, PV-cre, or SST cre-mice

(P50–55), which were injected with either AAV9-EF1α-DIO-ChETA-EYFP or AAV9-Syn-ChrimsonR-tdT. Standard methods of slice preparation were used (Suzuki and Bekkers 2006, 2011). Briefly, sagittal slices of the APC (300 μm thick) were prepared in ice-cold slicing solution containing (in mM) 110 Choline-Cl, 2.5 KCl, 0.5 $CaCl_2$, 10 $MgSO_4$, 1.25 NaH_2PO_4, 24 $NaHCO_3$, and 20 glucose. Slices were used for recording following a recovery period of 1 h at room temperature.

2.4 | Electrophysiology and data analyses

Recordings were performed and continuously superfused at 2–3 ml/min in artificial cerebrospinal fluid (ACSF) containing 119 NaCl, 2.5 KCl, 2.5 $CaCl_2$, 1.3 $MgSO_4$, 1 NaH_2PO_4, 26.2 $NaHCO_3$, and 22 glucose that is saturated with 95% O_2 and 5% CO_2 (carbogen) at room temperature. The microscope (Nikon Eclipse FN1) was equipped with wide-field LED to enable patterned illumination of field of view (FOV) in labeled neurons. Slices were oriented such that L1 faces the top with L3 facing the bottom of the FOV, with L2 right in the center. Since a continuum exists between the superficial L2a SL and deeper L2b SP cell types,[13] we recorded from cells that were at the extreme ends of L2, that is, closer to L1/L2a border for SL, and L2b/L3 border for SP, cells (Figure 1A,B). Recording pipettes were pulled from borosilicate glass (Harvard Apparatus) and open-tip resistance was typically 4–6 MΩ. Recordings were obtained from neurons using whole-cell patch-clamp technique with an internal solution that is based either on Cs^+ gluconate: (in mM) 130 D-gluconic acid, 130 CsOH, 5 NaCl, 10 HEPES, 12 Di-Tris-P-creatine, 1 EGTA, 3Mg-ATP, and 0.2 Na-GTP (pH 7.3; 290 mOsm) or K^+ gluconate (components are the same except that 130 mM Cs^+ gluconate was replaced by K^+ gluconate). Unless stated otherwise, all compounds were obtained from Sigma-Aldrich. For recordings of EPSCs or IPSCs, cells were held at holding potentials (V_h) of −70 or +10 mV respectively. We did not compensate for junction potential. For Chrimson experiments, we looked for the main injection site where it showed Chrimson+ cell bodies and moved laterally at least 500 μm away (typically 700–1000 μm) where there were only Chrimson+ axons but not cell bodies. Chrimson+ neurons and axons were activated by yellow-green light illumination (560 nm; 100% power was ~170 mW measured at the output of the liquid light guide; X-Cite XLED1). Brief (1–10 ms) pulses of LED light was focused on to the back aperture of objective (Nikon FN1) for whole-field illumination (controlled via NI PCIe-6321 NIDAQ card). Care was taken to avoid direct dendritic stimulation, which was indicated as spikes with <2 ms response onset latency. For CheTA experiments, we recorded from the injection site where there was a large number of CheTA+ PV/SST cell bodies. ChETA was activated by brief pulses of blue LED light (470 nm; 100% power was ~1.5 W measured at the output of the liquid light guide). Selective illumination was achieved by restricting LED illumination to L1, L2, or L3 using a digital mirror device (DMD; Mightex Polygon400) in series with the epifluorescent light path of liquid light guide output. A rectangular area containing L1 or L3 were hand-drawn for specifying the illumination area (Nikon NIS-Elements Ar) viewed through a water-immersion, 40× objective (Nikon CFI Apo 40×W NIR, NA 0.8; Figure 2). For LFP recordings, a pipette filled with ACSF was placed in the middle of L1 or L3 to record current sinks or sources in current clamp ($I = 0$) mode. For firing-current injection experiments, the cell was allowed to remain at its resting membrane potential and recorded in current-clamp mode. A series of current steps (duration 500 ms, amplitudes ranging from −50 to 510 pA in increments of 40 pA) was applied to identify neuronal firing patterns. Series resistance (<25 MΩ; uncompensated) was regularly monitored during recordings, and cells were rejected if resistance changed >20% during the experiment. Data were filtered at 2 kHz, digitized at 5–10 kHz, acquired through Multiclamp 700B, Digidata 1550B1, and pCLAMP 10 (Molecular Devices). As inhibition in APC exhibits a rostral-caudal gradient in that inhibition is stronger in the caudal APC[21,24] and odor responses differ between rostral and caudal APC,[25] we were vigilant in (1) making sure that we were always recording from the most rostral part of APC, and (2) most of the recorded SL and SP cell pairs were in the same slice and had roughly equal distance between slices. Hence, recordings were mostly made from sequential pairs in the same slice. Response latency was measured from light onset to when the response was clearly above the baseline. The largest amplitude was used for response amplitude.

2.5 | Computation of synaptic conductance

EPSCs are predominantly mediated by AMPA receptors, which are largely permeable to Na^+ and K^+ ions with negligible permeability for Ca^{2+}. With our best effort, however, we did not find evidence in the literature about the reversal potential properties of AMPA receptors in the APC. Hence, we assume that the reversal potential and ionic permeability properties of AMPA receptors in APC are similar to those in hippocampal CA1.[26] Using ionic concentrations of Na^+, K^+, Ca^{2+}, and Cl^- in our ACSF and internal solution, we computed the E_{rev} for glutamate

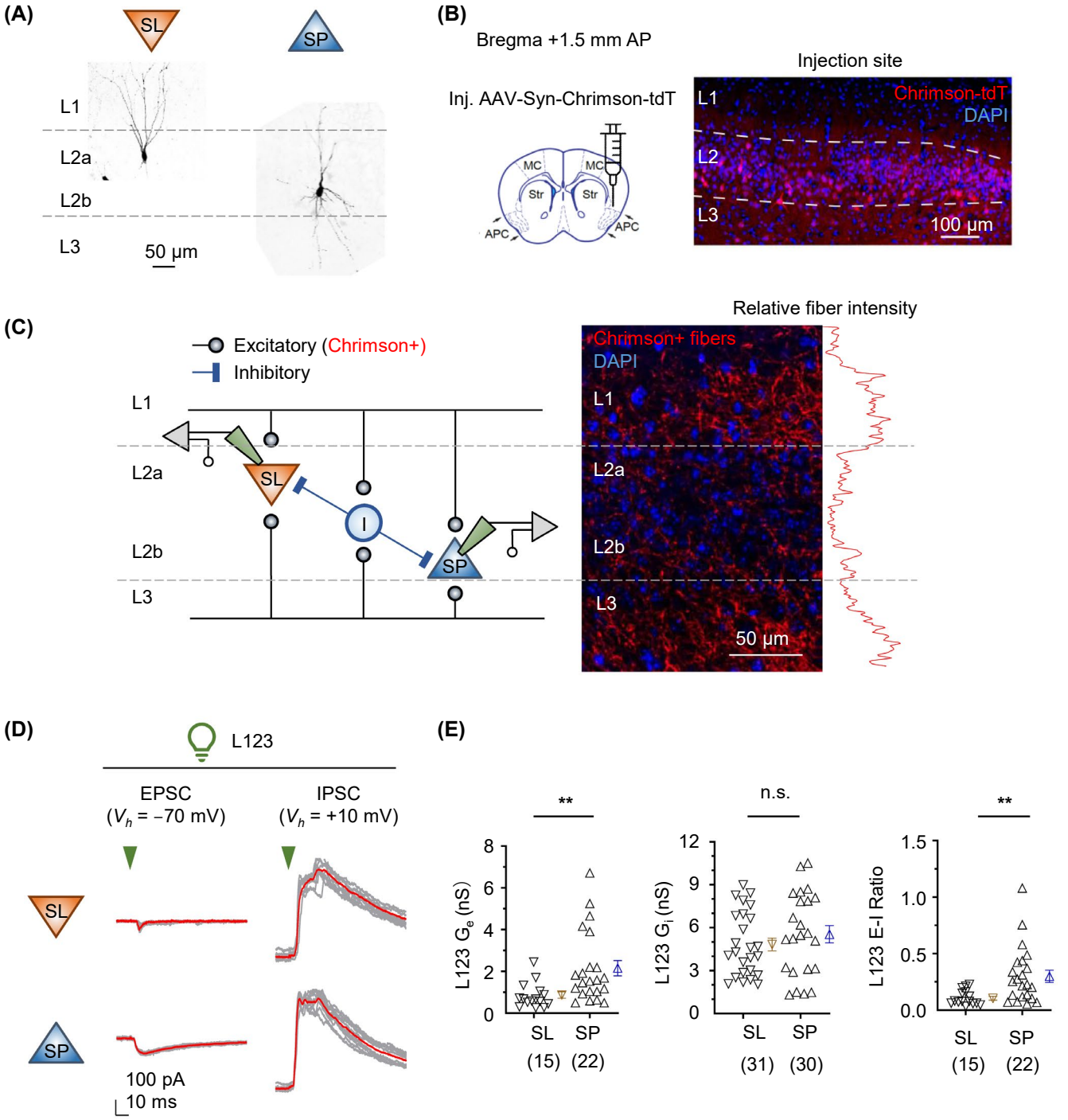

FIGURE 1 Identification of L2 principal neurons, SL and SP cells, in APC. (A) Representative, maximum-intensity projection images of filled SL and SP cells. The SL cell (recorded from L2a) showed more dendrites emanating from the cell body into the L1, whereas SP cell (recorded from L2b) showed more basal dendrites extending into L3. L1, layer 1; L2, layer 2; L3, layer 3. (B) Confocal image showing cell body expression of Chrimson-tdT in the injection site. AP, anterior-posterior coordinates relative to bregma; MC, motor cortex; Str, striatum; APC, anterior piriform cortex. (C) Schematic of recording of SL and SP cells (left) where only fibers were detected but cell bodies were Chrimson-negative (1 mm away from injection site; right). (D) Representative traces of EPSCs (V_h = −70 mV) and IPSCs (V_h = +10 mV) triggered by whole-field illumination of APC (L123; 1 ms pulse width) in SL versus SP cells. Grey, 10 superimposed individual trial traces; red, mean traces. (E) EPSC conductance (G_e) was much higher in SP compared to SL cells (SL vs. SP, 0.83 ± 0.15 vs. 2.12 ± 0.36 nS, n = 15 vs. 22, p = .003), while disynaptic/polysynaptic IPSC conductance (G_i) was equally strong (SL vs. SP, p = .161), leading to a higher E–I ratio in SP cells (SL vs. SP, 0.11 ± 0.02 vs. 0.31 ± 0.05, n = 15 vs. 22, p = .003)

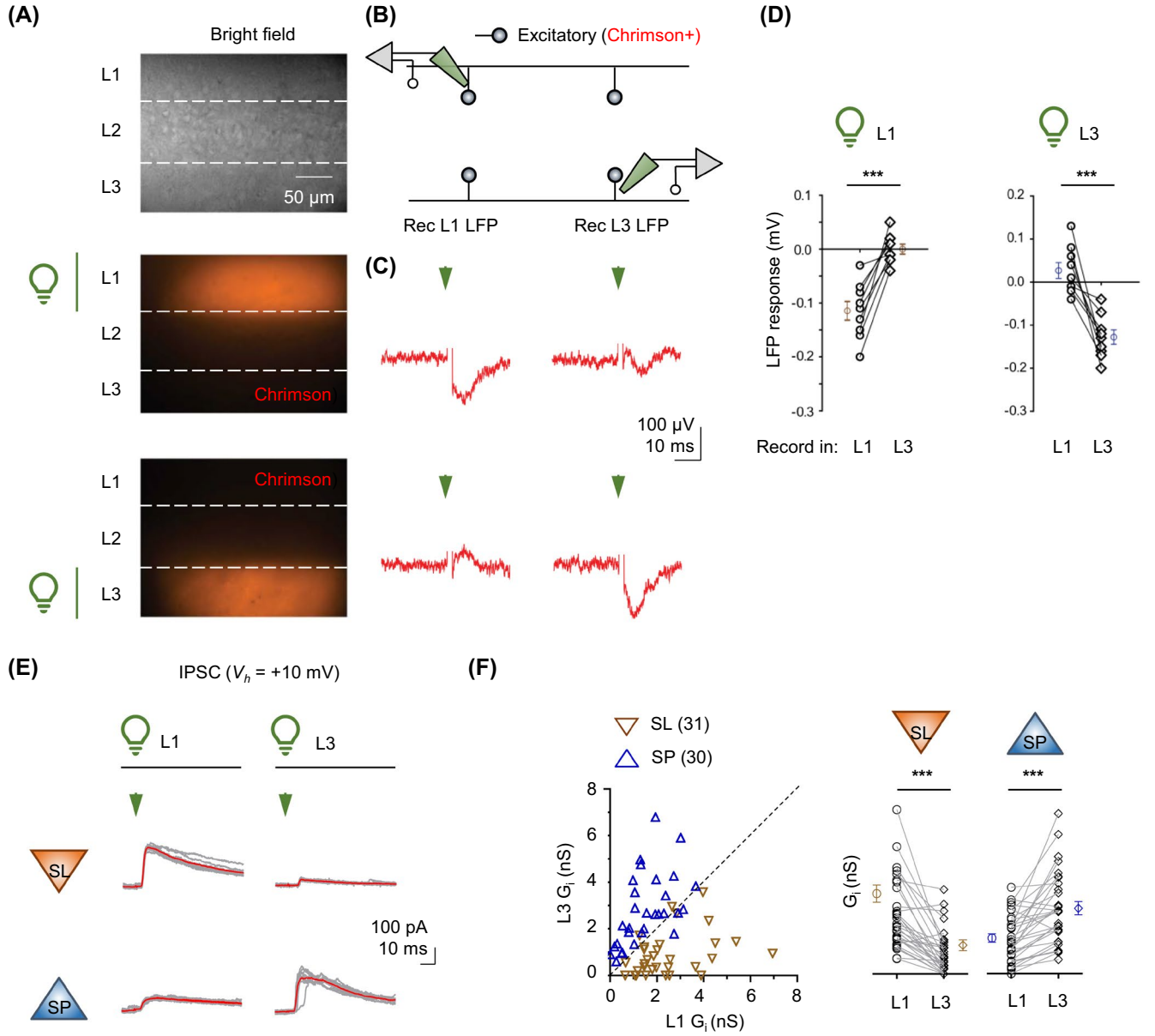

FIGURE 2 Optogenetic stimulation of specific layers revealed target-specific connectivity of recurrent inhibition. (A and B) Bright-field image of the APC brain slice and fluorescent image of the fibers (A) with a schematic of the local field potential (LFP) recording site (40× objective; B). Patterned illumination of L1 or L3 using 560 nm excitation (2 ms) showed that light was spatially restricted to the marked layers. (C and D) Representative traces (C) and summary data (D) showing that excitatory responses were largely confined to the activated layers (stimulating L1, recording L1 vs. L3: −0.11 ± 0.02 vs. 0.0 ± 0.01, $n = 9$, $p = .0002$; stimulating L3, recording L1 vs. L3: 0.02 ± 0.01 vs. −0.13 ± 0.02, $n = 8$, $p = .0008$). Stimulus artifact was removed for simplicity. (E and F) Representative traces (E) and summary data (F) showing that L1 inhibition was stronger in SL cells whereas L3 inhibition was stronger in SP cells (SL, L1 vs. L3: 2.49 ± 0.27 vs. 0.89 ± 17 nS, $n = 31$ cells, $p < .001$, paired t-test; SP, L1 vs. L3: 1.53 ± 0.18 vs. 2.79 ± 0.28 nS, $n = 30$ cells, $p < .001$, paired t-test)

(E_e) using the Goldman-Hodgkin-Katz equation (https://www.physiologyweb.com/calculators/ghk_equation_calculator.html):

$$V_m = \frac{RT}{F} \ln \left(\frac{p_K[K^+]_0 + p_{Na}[Na^+]_0 + p_{Cl}[Cl^-]_i}{p_K[K^+]_i + p_{Na}[Na^+]_i + p_{Cl}[Cl^-]_0} \right).$$

where T = 298 K, $p_K = 1$, $p_{Na} = 0.84$, $p_{Cl} = 0.02$, $[K^+]_0$ = 2.5 mM, $[K^+]_i$ = 130 mM, $[Na^+]_0$ = 146.2 mM, $[Na^+]_i$ = 5.2 mM, $[Cl^-]_0$ = 126.5 mM, $[Cl^-]_i$ = 5 mM, V_m = −70 mV.

At room temperature (298 K), $E_e = -2.3$ mV.

IPSCs are predominantly mediated by GABAA receptors, which lets Cl^- permeate. Using ionic concentrations of Cl^- in our ACSF and internal solution, we computed the reversal potential for GABA (E_i) using the Nerst equation (https://www.physiologyweb.com/calculators/nernst_potential_calculator.html):

$$V_{\text{Eq.}} = \frac{RT}{zF} \ln\left(\frac{[X]_{\text{out}}}{[X]_{\text{in}}}\right).$$

At room temperature (298 K), $E_i = -83.0$ mV.

We displayed our data in the form of peak synaptic conductance (G, in nS) instead of peak current amplitude (in pA). We computed the excitatory synaptic conductance G_e and inhibitory synaptic conductance G_i using the following Equation[27]:

$$G_e = I_e / \left(V_e - E_e\right) \text{ where } V_e = -70 \text{ mV and } E_e = -2.3 \text{ mV}$$

$$G_i = I_i / \left(V_i - E_i\right) \text{ where } V_i = +10 \text{ mV and } E_i = -83 \text{ mV}$$

where V_e and V_i are the clamping voltage for recording EPSC and IPSC, respectively; E_e and E_i are the reversal potentials of the excitatory and inhibitory synaptic conductances, respectively; and I_e and I_i are the amplitude of the EPSC and IPSC respectively.

2.6 | Immunofluorescent staining and filled-cell imaging

PV-cre or SST cre-mice (P49–56), which were injected with AAV9-EF1α-DIO-ChETA-EYFP into APC were anesthetized and fixed by transcardial perfusion with 4% formaldehyde. Floating sagittal APC sections (100 μm) were prepared (Leica VT1000S). Sections were blocked with PBS containing 5% normal goat serum and 0.1% Triton X-100 and were incubated with an antibody against PV (1:1000, rabbit or mouse, Swant), or SST (1:500, Santa Cruz) overnight at 4°C. Sections were decorated with secondary antibody conjugated with Alexa 488 or 568 dye and mounted in VectaShield (Vector Labs). Images of CheTA expression were acquired with a confocal microscope (Zeiss LSM 880 Airyscan) using a 40×, 1.3 NA oil-immersion or 10× air objective using a pinhole of 1 Airy unit (488 nm Ex and 505–530 nm Em). Fluorescence of Chrimson-tdtomato was imaged using 543 nm Ex/560–615 Em. To image the morphology of recorded SL and SP cells, cells were filled by including biocytin (2 mg/ml, TRC, Canada) in the internal solution and recording in whole-cell mode for at least 15 min. Slices were then fixed overnight with 4% formaldehyde, permeabilized with 0.1% Triton X-100 and stained with streptavidin-Alexa Fluor 594 (Life Technologies). Cells were imaged with the above microscope at 10× air using Z-stacks (2 μm step size; 543 nm Ex/560–615 Em or 561 nm Ex/595–645 nm Em). Maximum intensity projections were used to illustrate the morphology of SL or SP cells.

2.7 | Experimental design and statistical analyses

For electrophysiology, spike frequency, EPSC and IPSC amplitudes were analyzed using PCLAMP or custom-written scripts in MATLAB (MathWorks). Unless noted otherwise, data were analyzed with paired t-test (if distributions are normal) or Mann–Whitney U-test, one-way analysis of variance (ANOVA) with Tukey's test for multiple comparisons and presented as mean ± SEM (n is the number of recorded cells). Significance was indicated if $p < .05$. Power analysis: for a t-distribution with mean of μ and standard deviation of 10% of μ, to detect a 10% change in mean with 0.8 power $(1 - \beta)$ we estimated that we needed an n of 10 animals for each condition. The numbers displayed between parentheses within figures represent the number of recorded cells.

3 | RESULTS

3.1 | Differential inhibitory transmission in SL and SP cells in APC

To examine whether there was any fundamental difference between the inhibition received by SL versus SP cells, we recorded adjacent neurons in L2a (SL-like cells) and L2b (SP-like cells) in acute brain slices of mouse APC (Figure 1A). Compared to SL cells, SP cells showed lower input resistance and higher capacitance (SL vs. SP, 374.0 ± 83 vs. 201.6 ± 24 MΩ; 26.2 ± 4.1 vs. 40.0 ± 3.5 pF, $n = 9$ vs. 15, $p = .03$ for both), had one main dendritic trunk emanating from the cell body, and showed more basal dendrites, corroborating with previous findings.[13] Having verified that we were able to distinguish SL from SP cells using layer position, passive membrane properties and morphology, we recorded sIPSCs from these two neuron types. sIPSC in SL and SP cells were of similar inhibitory conductance (G_i; SL vs. SP, 0.26 ± 0.01 vs. 0.24 ± 0.01 nS, $n = 89$ vs. 75, $p = .135$) but showed significantly higher frequency in SL cells (SL vs. SP, 4.3 ± 0.2 vs. 3.1 ± 0.1 Hz, $n = 89$ vs. 75, $p < .001$). The left and right APC did not differ in the above parameters, and we pooled these data. These experiments established that the inhibitory circuits were differentially wired up for SL and SP cells.

3.2 | Laminar- and target-specific connectivity of recurrent inhibitory circuits

sIPSC can offer an overview of synaptic inhibition received by SL and SP cells, but does not reveal whether

evoked excitation and inhibition differ in these principal neuron types. The axons of principal neurons extend laterally along the APC; activation of these axons constitute recurrent excitation. This recurrent excitation then activates interneurons to impart local, recurrent inhibition. A traditional method of examining recurrent pathways is to place stimulating electrodes in various layers to selectively monitor them, but electrode placement and stimulation intensity are highly variable. To activate the maximum number of fibers and reduce variability, we used optogenetics that offers good spatial and temporal stimulation control. To assess the recurrent excitation–inhibition (E–I) ratio received by SL and SP cells, we expressed the red-shifted Channelrhodopsin, Chrimson, by stereotaxic injection into the APC (Figure 1B). Expression of Chrimson was driven by the synapsin promoter, and hence both excitatory and inhibitory neurons expressed it. Chrimson was robustly expressed in the APC, as revealed by confocal imaging of the neuron cell bodies and projection fibers (Figure 1B,C). It is mainly the excitatory neurons extend their axons over millimeters, whereas the axons of inhibitory neurons ramify locally (hundreds of microns). Moving ~1 mm away from the injection site, we recorded from Chrimson-negative L2 principal neurons, where Chrimson-positive fibers coalesced mainly in L1 and L3 (Figure 1C). Whole-field illumination (L123, 560 nm, 1 ms pulse width) of APC triggered recurrent EPSCs (V_h = −70 mV) and IPSCs (V_h = +10 mV) in principal neurons (Figure 1D). SP cells received robust EPSCs with strong excitatory conductance (G_e) while SL cells received much weaker or no EPSCs (Figure 1D,E), corroborating previous reports.[21,28] Similar to a published report,[6] application of CNQX (10 μM) and D,L-APV (100 μM) blocked both EPSCs and IPSCs, indicating that these are synaptic currents rather than self-stimulation of Chrimson + cells (data not shown). In contrast with EPSC, both SL and SP cells received strong disynaptic/polysynaptic IPSCs that were comparable in magnitude (Figure 1E). Both EPSCs and IPSCs were reliable as indicated by the superimposed per-trial (grey) and mean (red) traces (Figure 1D). Hence, the E–I ratio was significantly higher in SP cells (Figure 1E).

Our previous experiment activated all recurrent excitation and inhibition in the field. However, recurrent excitatory fibers coalesce mainly in L1 and L3 (Figure 1B) and can elicit different excitation and inhibition either via the L1 or L3 subset of fibers.[21] To understand the relative contribution of L1 versus L3 input, we used patterned illumination by inserting a digital mirror device (DMD) in-series with the LED light source, which allowed us to reliably and maximally activate the top third (L1) or bottom third (L3) in the same slice while recording local field potentials (LFPs) in either L1 or L3 (Figure 2A,B). Using this method, we observed negative deflection in LFP only in the layer that was activated, that is, response in L1 when L1 but not L3 was stimulated, and vice versa for L3 response (Figure 2C,D). This suggests that excitatory synaptic activity was largely confined to its respective layers of presynaptic fibers. Does the recurrent inhibition arising from L1 or L3 differ for SL versus SP cells? We next recorded IPSCs from sequential pairs of neighboring SL and SP cells while illuminating either L1 or L3. Here, we revealed differential, target-specific inhibitory wiring: SL cells received stronger inhibition from L1, whereas SP cells received stronger inhibition from L3 (Figure 2E). Plotting L1 against L3 IPSC conductance, SL data points largely lied beneath, whereas SP data points largely lied above, the unity line (Figure 2F). This indicates that there is a higher tendency for recurrent inhibition from L1 to target SL cells, while there is a higher tendency for inhibition from L3 to target SP cells. Consistent results were obtained by (1) normalizing layer-specific responses to whole field illumination (all of L123), or (2) analyzing IPSC amplitudes after removal of trials with no responses (data not shown). These results strongly suggest that inhibitory circuits are wired up with laminar specificity for the two major principal neuron types: recurrent inhibition exhibits opposite pattern of connectivity for SL versus SP cells depending on which layer is activated.

3.3 | Target-specific connectivity of PV and SST interneuron circuits in APC

Recurrent inhibition is mediated by a variety of GABAergic interneurons in the APC.[29] The PV- and SST-expressing interneurons are two major subtypes that provide local inhibition in the APC. Do PV and SST interneurons differentially target the L2 principal neurons? The PV neuron imparts potent inhibition owing to its strong, perisomatic synapses and high firing rate.[30] To examine the contribution of PV neurons, we expressed a channelrhodopsin with fast kinetics, ChETA, in APC of PV-Cre mouse.[31] CheTA + PV cell bodies were abundant in L3, with some residing in L2 and, in a small amount, L1, corroborating with a previous finding (Figure 3A).[32] Whole-field illumination of L123 (470 nm, 10 ms) showed that both SL and SP cells were highly connected with PV neurons, as shown by a 100% connectivity for both neuron types (Figure 3B). SP cells received PV inhibition that was twice as strong compared to SL cells (Figure 3B–D). These results show that PV neurons innervate both L2 principal neurons with high probability with overall stronger synaptic strength on to SP cells.

In addition to PV interneurons, the SST interneuron is another major interneuron subtype that provides broad

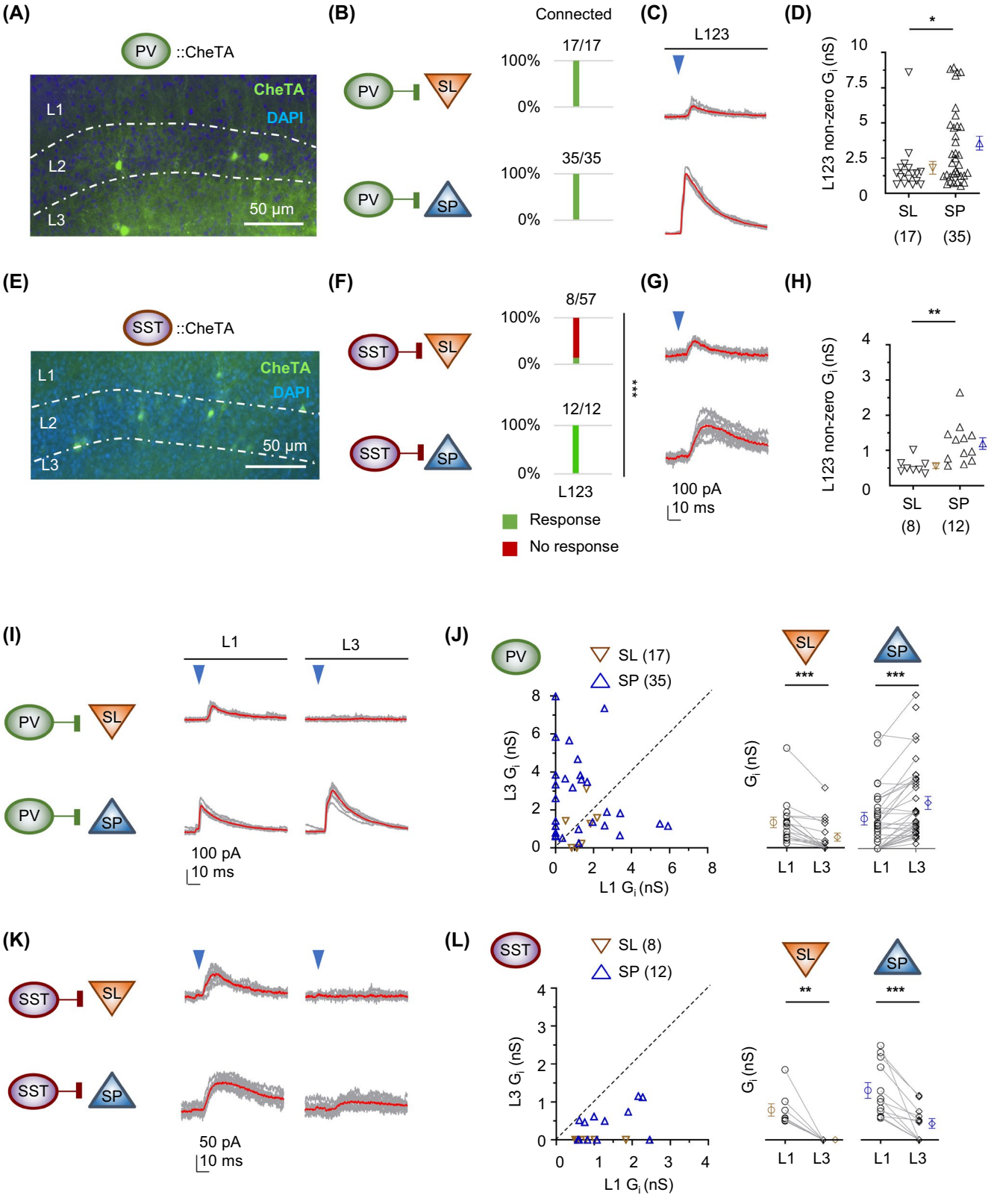

inhibition on both interneurons and pyramidal cells in APC.[33] L3 pyramidal cells in APC receive inhibition from SST-interneurons,[34] but it is unclear whether and how SST interneurons can differentially regulate SL and SP cells in a target-specific manner. We examined SST output to SL and SP cells by expressing ChETA in APC of SST-Cre mice (Figure 3E). Overall, SST output to SL cells was far weaker than to SP cells because only 14% (8/57) of SL cells (compared to 100% [12/12] for SP cells) had an SST response ($p = 1.4 \times 10^{-8}$, Fisher's exact test). We next quantified the

FIGURE 3 PV interneuronal output exhibited the same laminar- and target-specific connectivity as recurrent inhibition. (A) Epifluorescent image of ChETA-EYFP expression in APC of PV-cre mice (PV::CheTA). (B–D) Circuit schematic and number of connected cells (B), representative traces (C) and summary data (D) of evoked, PV-mediated IPSC performed with whole-field illumination. PV neurons output to SL and SP cells with high probability (100%), with a preference for SP cells. (E–H) The same experiments above repeated in the SST-Cre mice. SST neurons connected with SL cells with low probability (8/57 or 14%) and SP cells with high probability (100%). When connected, SST output to SL cells were weaker than for SP cells. Using only cells that had responses (non-zero responses), SP cells received stronger response from both PV and SST output compared to SL cells (PV vs. SST → SL, 1.77 ± 0.45 vs. 0.55 ± 0.07 nS, $n = 17$ vs. 8, $p < .001$; PV vs. SST → SP, 3.53 ± 2.95 vs. 1.20 ± 0.17 nS, $n = 35$ vs. 12, $p = .007$). (I and J) Patterned illumination of L1 or L3 showed PV-mediated inhibitory output was stronger in L1 than L3 in SL cells (L1 vs. L3, 1.31 ± 0.28 vs. 0.54 ± 0.21 nS, $n = 17$ cells, $p < .001$) but was stronger in L3 than L1 in SP cells (L1 vs. L3, 1.53 ± 0.33 vs. 2.37 ± 0.34 nS, $n = 35$ cells, $p < .001$). (K and L) In contrary with PV inhibition, SST-mediated output was stronger in L1 than L3 for both SL cells (L1 vs. L3, 0.78 ± 0.16 vs. 0 ± 0 nS, $n = 8$ cells, $p = .002$) and SP cells (L1 vs. L3, 0.84 ± 0.21 vs. 0.43 ± 0.13 nS, $n = 12$ cells, $p < .001$). Data analyzed with paired t-test, mean ± SEM. *$p < .05$, **$p < .01$, ***$p < .001$

non-zero responses in SL and SP cells. When connected, the non-zero responses in SL cells were half as strong as in SP cells (Figure 3F–H). Comparing the grouped data for PV → SL/SP versus SST → SL/SP, PV connectivity was significantly higher than that for SST neurons ($p = 6 \times 10^{-18}$, Fisher's exact test) and that its connected strength was approximately three times higher (PV vs. SST, 2.95 ± 0.38 vs. 0.94 ± 0.13 nS, $n = 52$ vs. 20, $p < .001$). Overall, these data suggest that PV output is much stronger than that of SST output in the APC.

Do PV and SST neuronal output exhibit laminar and target specificity? To address this, we dissected the laminar specificity of PV inhibition by performing patterned illumination of L1 or L3 as above (Figure 2). SL cells received stronger PV inhibition from L1 compared to L3 (Figure 3I,J). In stark contrast, SP cells received stronger PV inhibition from L3 compared to L1 (Figure 3I,J). Taken together, these results reveal an important connection motif: PV output to SL versus SP cells exhibits opposite pattern of laminar connectivity. Importantly, the organization of PV output circuit matches that of activation of recurrent inhibition (Figure 2).

Next, we dissected the laminar specificity of SST output using patterned illumination as above. In contrary with PV inhibition, SST output to both SL and SP cells exhibited the same laminar specificity: stronger in L1 than L3 (Figure 3K,L). In summary, here we reveal a laminar- and target-specific connectivity for interneuron subtypes. PV output exhibits opposite laminar connectivity with SL versus SP cells; SST output exhibits same laminar connectivity for both SL and SP cells.

3.4 | Activity deprivation differentially altered inhibitory synaptic transmission in SL versus SP cells

In the APC, olfactory discrimination learning modulates synaptic strength that is pathway-dependent,[35] but whether SL and SP cells display differential plasticity is unknown. Owing to how SL and SP cells can be activated by direct OB versus associational pathways and that the two pathways exhibit different long-term synaptic plasticity,[5] we hypothesized that specific inhibitory circuits respond with different plasticity rules. To examine this, we subjected mice to naris occlusion (NO), recorded sIPSCs from SL and SP cells, and compared the open and occluded APCs (Figure 4A). NO did not detectably alter the conductance or frequency of sIPSCs in SL cells (Figure 4A–C). By contrast, NO significantly upregulated the conductance, but not frequency, of sIPSCs in SP cells (Figure 4A–C). These results suggest the possibility that activity deprivation drives SP cell-specific plasticity.

3.5 | Naris occlusion differentially regulated plasticity of recurrent inhibition in SL versus SP cells

Does sensory activity differentially modulate recurrent inhibitory circuits that control SL and SP cells? We examined recurrent excitation and inhibition using Chrimson labeling of recurrent pathway and compared open versus occluded APC. NO selectively enhanced the recurrent IPSC conductance in SP but not in SL cells through whole-field (L123) stimulation (SP, to 145 ± 14%, $p = .019$; SL, 121 ± 11% $p = .16$; Figure 5A,B), consistent with the increased sIPSC conductance for SP cells (Figure 4). For SP cells, is the locus of IPSC enhancement in L1 or L3? Selective stimulation of L1 versus L3 revealed that NO did not alter the IPSC conductance in either L1 or L3 for SL cells (Figure 5C,D), similar to whole-field illumination (Figure 5A,B). By contrast, NO significantly increased IPSC conductance in SP cells in both L1 and L3 while preserving the laminar specificity (L1, to 166 ± 23%, $p = .035$; L3, to 200 ± 23%, $p = .002$, L1 < L3; Figure 5E,F) as seen in naïve animals (Figure 2). These results indicate that plasticity of inhibition occurs in a laminar- (L3) and target- (SP cell) specific manner.

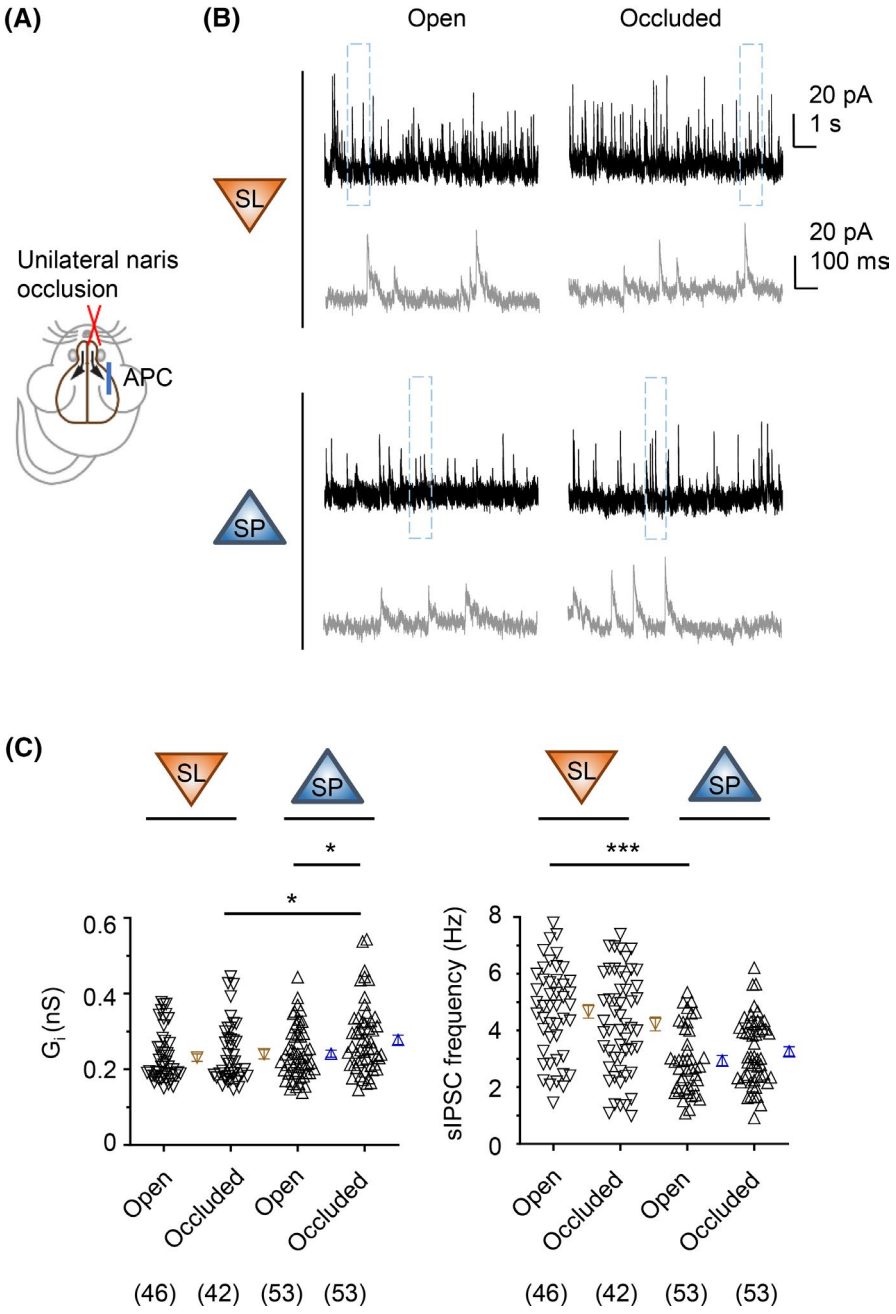

FIGURE 4 Naris occlusion augmented the conductance of spontaneous IPSCs in SP cells only. (A) Schematic showing unilateral naris occlusion (NO) blocked activity on one side of APC. (B–C) Representative traces (B) and summary data (C) showing that NO did not detectably alter the conductance or frequency of sIPSCs in SL cells (open vs. occluded: conductance, $p = .36$; frequency, $p = .23$), but significantly upregulated the conductance, not frequency, of sIPSCs in SP cells (open vs. occluded, conductance, 0.24 ± 0.09 vs. 0.28 ± 0.01 nS, $n = 53$ vs. 53, $p = .023$; frequency, $p = .218$, Mann–Whitney test, mean ± SEM). *$p < .05$, **$p < .01$, ***$p < .001$

3.6 | Naris occlusion differentially regulated PV-mediated synaptic output in SL and SP cells

Our results thus far demonstrate that plasticity occurs specifically in the inhibitory circuit regulating the SP cell. Is this inhibitory plasticity mediated by specific interneuron subtypes? As PV output was stronger than that of SST (Figure 3), we first examined whether sensory experience regulated PV output by recording from SL versus SP cells while stimulating CheTA+ PV cells in open versus occluded APC (Figure 6A). There was no qualitative difference in cell bodies showing PV::CheTA expression after NO (data not shown). NO significantly enhanced

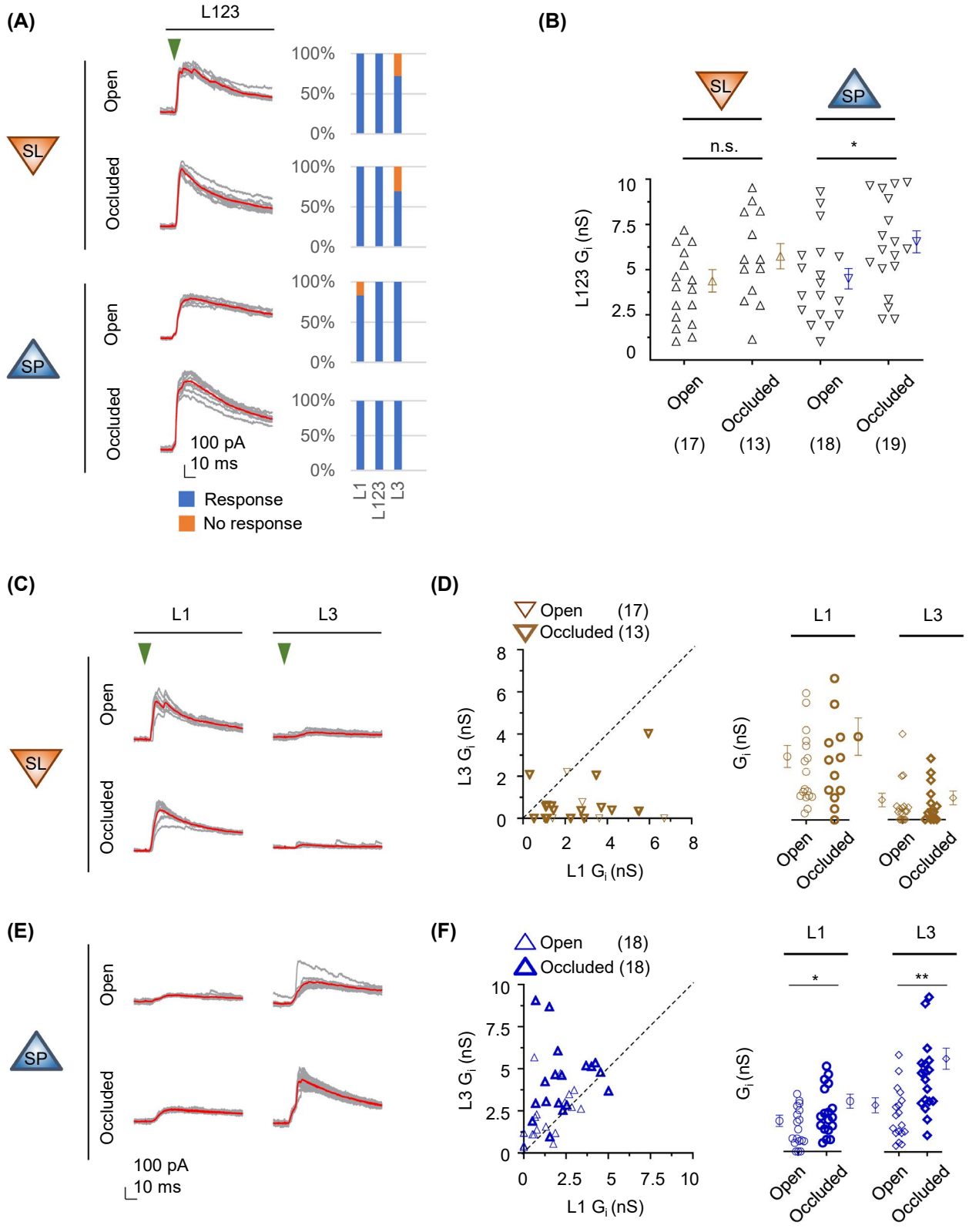

FIGURE 5 Naris occlusion selectively enhanced recurrent inhibition in SP cells. (A and B) Representative traces (A) and summary data (B) showing that NO significantly increased evoked L123 IPSC conductance in SP but not in SL cells (SP, open vs. occluded: 4.47 ± 0.57 vs. 6.51 ± 0.61 nS, $n = 18$ vs. 19, $p = .019$; SL, open vs. occluded: 4.35 ± 0.62 vs. 5.71 ± 0.70 nS, $n = 17$ vs. 13, $p = .16$). (C–F) Representative traces (C and E) and summary data (D,F) showing that NO did not alter IPSC conductance of SL in either L1 or L3 (L1, open vs. occluded, 2.36 ± 0.41 vs. 3.10 ± 0.70 nS $n = 17$ vs. 13, $p = .46$; L3, open vs. occluded: 0.74 ± 0.26 vs. 0.81 ± 0.26 nS, $n = 17$ vs. 13, $p = .87$), but significantly increased IPSC conductance of SP cells in both L1 and L3 (L1, open vs. occluded: 1.41 ± 0.26 vs. 2.34 ± 0.33 nS, $n = 18$ vs. 18, $p = .034$; L3, open vs. occluded: 2.19 ± 0.35 vs. 4.37 ± 0.50 nS, $n = 18$ vs. 18, $p = .002$). Data were analyzed with Mann–Whitney test, mean ± SEM. *$p < .05$, **$p < .01$, ***$p < .001$

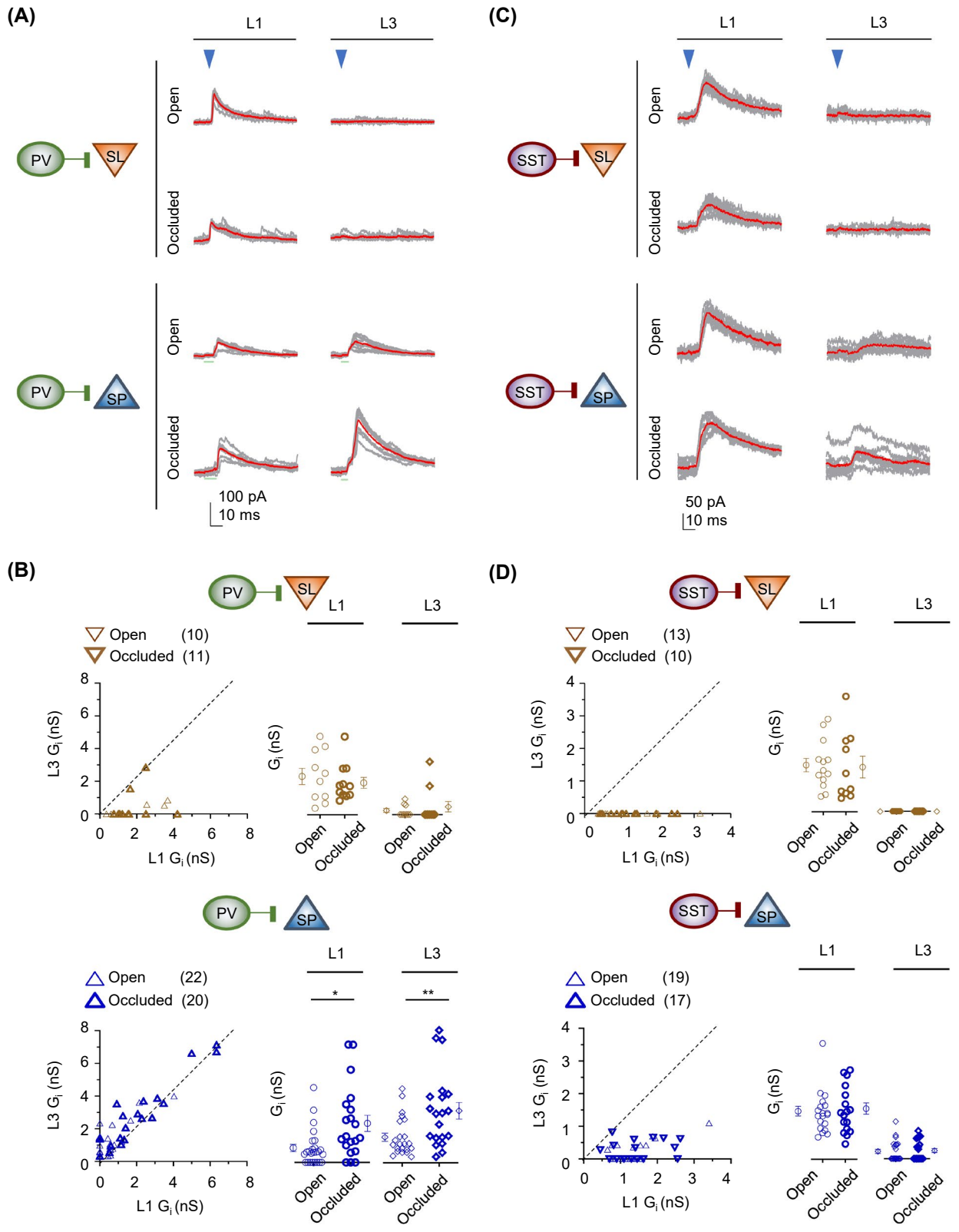

FIGURE 6 Naris occlusion selectively enhanced PV inhibition in SP cells. (A and B) Representative traces (A) and summary data (B) showing NO enhanced PV-mediated IPSC conductance in SP cells arising in both L1 and L3 (L1, open vs. occluded: 0.77 ± 0.19 vs. 2.11 ± 0.43 nS, $n = 22$ vs. 20, $p = .013$; L3, open vs. occluded: 1.41 ± 0.22 vs. 2.83 ± 0.45 nS, $n = 22$ vs. 20, $p = .009$; B) but not in SL cells (open vs. occluded, L1, $p = .81$; L3, $p = .78$; $n = 10$ vs. 11). (C and D) NO did not alter SST-mediated synaptic output in either L1 or L3 for both SL and SP cells (open vs. occluded, SL, L1, $n = 13$ vs. 10, $p = .83$; L3, no response; SP, L1, $n = 19$ vs. 17, $p = .73$; L3, $p = .87$). Data were analyzed using Mann–Whitney test, mean ± SEM. *$p < .05$, **$p < .01$, ***$p < .001$

whole-field conductance of PV IPSC in SP but not SL cells (SL, open vs. occluded: 3.52 ± 0.60 vs. 2.30 ± 0.39 nS, $n = 10$ vs. 11, $p = .11$; SP, open vs. occluded: 2.39 ± 0.29 vs. 3.56 ± 0.46 nS, $n = 22$ vs. 20, $p = .042$). Further experiments using patterned illumination showed that NO significantly increased PV IPSC conductance in SP cells in both L1 and L3, suggesting that there was no laminar specificity for sensory plasticity (Figure 6B). The enhancement in PV → SP cell in both L1 and L3 is similar to the results for recurrent inhibition (Figure 5). Of note, the overall laminar specificity for both PV output was maintained in both the open and occluded sides (Figure 6A,B) compared to untreated control (Figure 3), suggesting this is an important circuit principle.

The increase in PV inhibition following activity deprivation could be due to enhanced intrinsic properties of PV cells. To examine whether NO enhanced PV output by altering its basic biophysical properties, we recorded from fluorescently identified L3 PV cells (CheTA+), injected direct currents and measured their excitability. NO did not detectably alter three properties of PV interneurons: maximal firing rate, resting membrane potential, and threshold current required to induce a spike (Figure 7). Together, these results indicate that NO enhanced synaptic inhibition originating from L3 PV neurons, which can largely explain the enhanced recurrent inhibition induced by NO.

3.7 | Naris occlusion did not alter SST-mediated synaptic output

Next, we examined the effects of activity deprivation on SST neuronal output. There was no qualitative difference in cell bodies showing SST::CheTA expression after NO (data not shown). NO did not detectably alter whole-field conductance of SST IPSC in SL or SP cells (SL, open vs. occluded: 1.10 ± 0.21 vs. 0.92 ± 0.17 nS, $n = 13$ vs. 10, $p = .64$; SP, open vs. occluded: 1.07 ± 0.09 vs. 0.98 ± 0.07 nS, $n = 19$ vs. 17, $p = .85$). NO did not alter SST-mediated synaptic output in both L1 and L3 for either SL or SP cells (Figure 6C,D). In both open and occluded sides, both SL and SP cells received stronger inhibition from L1 than L3 (Figure 6C,D). This laminar specificity is similar to that observed for the untreated control (Figure 3). Altogether, these results indicate a specific change in PV but not SST neuronal output following NO.

4 | DISCUSSION

More than a decade has passed since the electrophysiological characterization and distinction of two major principal neuron types in L2 APC, SL, and SP cells, but their specific roles in processing and learning of odor information remain elusive. Local inhibition is diverse and can selectively gate information in APC in a context-dependent manner, but the circuit mechanisms that enable this in the APC are unclear.

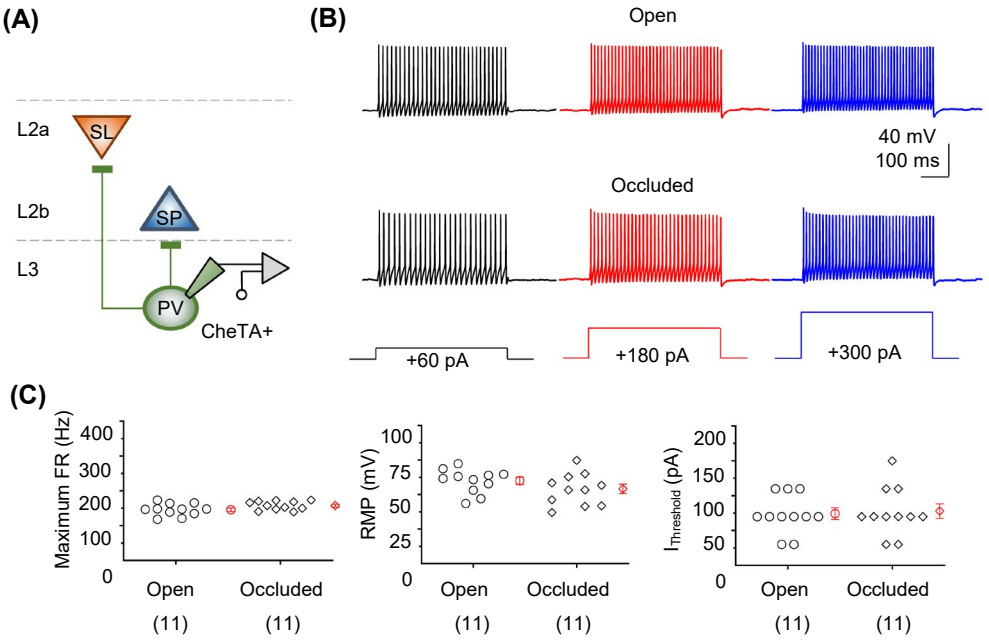

FIGURE 7 Naris occlusion did not alter L3 PV interneuron basic physiological properties. (A) Schematic recording of PV-interneurons (labeled by CheTA) in L3. (B) Representative trace of spikes in PV-interneurons following +60, +180, and +300 pA DC injection. (C) NO did not detectably alter the three properties of L3 PV interneurons: maximal firing rate (open vs. occluded, $n = 11$ vs. 11, $p = .082$), resting membrane potential (open vs. occluded, $n = 11$ vs. 11, $p = .19$), or threshold current required to induce a spike (open vs. occluded, $n = 11$ vs. 11, $p = .95$). Mann–Whitney test, mean ± SEM

Here, we made several important discoveries about the inhibitory circuits that regulate SL and SP cells. First, our data indicate that SL cells overall receives more inhibitory synaptic connections than SP cells, as shown by higher sIPSC frequency (Figure 1). Second, recurrent inhibition differed for SL versus SP cells: basally, SL cells received stronger inhibition from L1 while SP cells received stronger inhibition from L3 (Figure 2). Third, PV but not SST neurons strongly contribute to the layer-specific inhibition in SL versus SP cells (Figure 3). Interestingly, NO differentially regulated the two principal neuron types by increasing sIPSC conductance in SP cells only (Figure 4). NO further enhanced both L1 and L3 inhibition imparting on SP cells (Figure 5). This enhanced inhibition is contributed by PV, but not SST interneurons. (Figure 6) Taken together, we provide the first demonstration of layer- and target-specific connectivity of GABAergic neurons with principal neuron types in APC (Figure 8).

4.1 | Target-specific inhibition carried out by PV interneurons

Three lines of evidence converge on the notion that inhibitory circuits are differentially wired up for SL versus

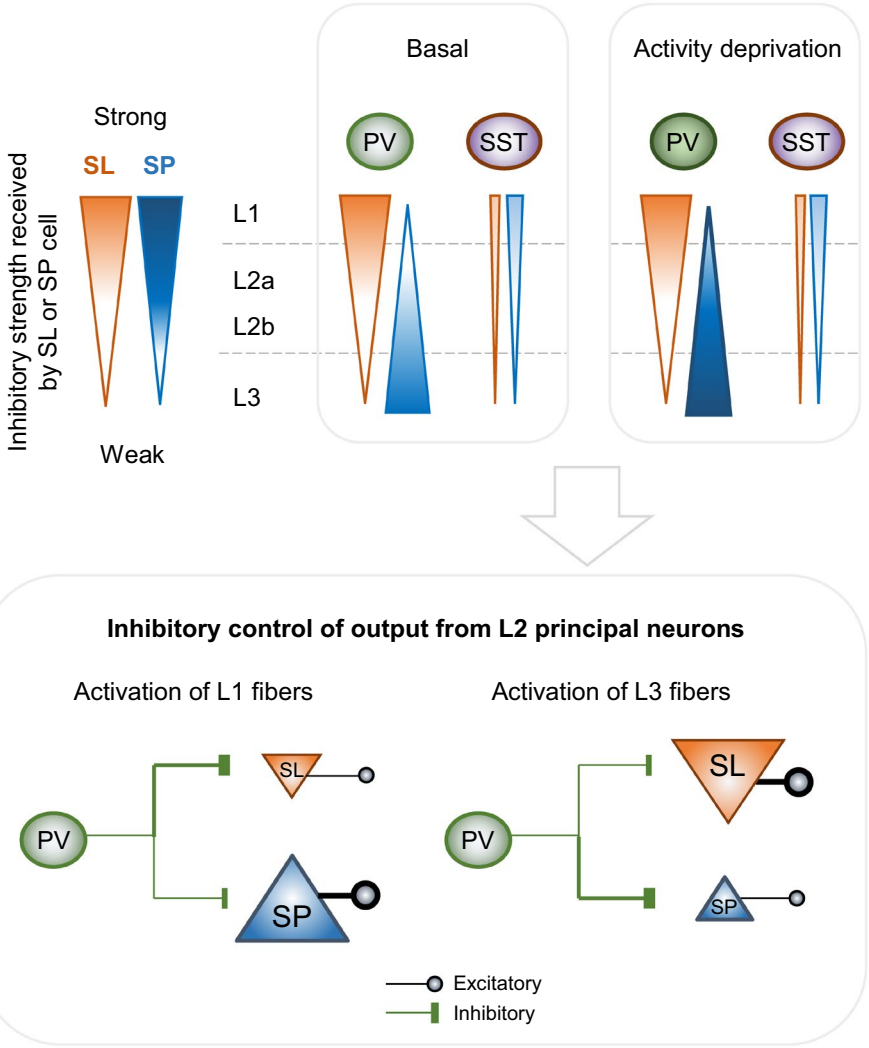

FIGURE 8 Schematic model of how laminar- and target-specific inhibitory connection can gate the output of piriform cortex. Under basal condition, PV interneurons mediate most of the recurrent inhibition, as the overall strength of PV inhibition is higher than that of SST. PV inhibition exhibits laminar- and target-specific connectivity in that it is L1 > L3 for SL (orange triangle), while L1 < L3 for SP cells (blue triangle). This implicates that activation of L1 recurrent excitation will recruit PV neurons to preferentially inhibit SL cells, while activation of L3 recurrent excitation can preferentially inhibit SP cells. In sharp contrast, SST inhibition is L1 > L3 for both SL and SP cells. Following activity deprivation, PV → SP inhibition (in both L1 and L3) is specifically enhanced. Despite all plastic changes, the overall differential laminar, and interneuron-principal neuron connectivity is preserved. Altogether, a physiological consequence of this laminar- and target-specific connectivity is that activation of L1 PV neurons can selectively suppress SL activity, while activation of L3 PV neurons can selectively suppress SP activity, gating the output of APC

SP cells. First, we found SL and SP cells exhibit opposite layer specificity in that inhibition originating from L1 is stronger for SL cells while inhibition originating from L3 is stronger for SP cells (Figure 2). This target and laminar difference is preserved even when NO alters inhibitory strength (Figure 5). In other words, the pattern that L3 inhibition is stronger than L1 for SP cells still holds. Theoretically, excitatory fibers in L1 could make a turn to or send a collateral to L3 and vice versa, muddling the L1 versus L3 specific responses. However, the fact that we consistently observed this layer specificity suggests that excitatory fibers do stay within their respective layers (Figure 2). As SP cells contain many more basal dendrites than SL cells,[13,14] it is possible that higher L3 recurrent inhibition (Figure 3C) could be due to the higher number of basal dendrites in SP cells. The relationship between EPSC and IPSC within a layer warrants further investigation.

Second, we showed that PV interneurons are largely responsible for this differential wiring and plasticity of SL versus SP cells. The pattern of PV inhibition being stronger in L1 for SL while it is stronger in L3 for SP cells (Figure 3) is consistent with the experiment performed with recurrent (Chrimson+) pathways (Figure 2). PV neurons in L3 are the multipolar, fast-spiking type that are similar to those found in the hippocampus and cortex, whereas those in L1 are more similar to horizontal interneurons.[29] As a published report[32] showed that a small fraction of PV cells residing in L1, our L1 specific illumination could be recruiting these PV cells. As such, L1 versus L3 PV neurons may not belong to the same interneuron subtype. Nevertheless, our experiments provide a robust, pairwise comparison between SL and SP cells because we activated the same sets of interneurons using patterned illumination in the same slice.

Third, we found that SL and SP cells have similar laminar specificity for SST output: stronger in L1 compared to L3. SST somata are in L3 while axons should be generally in L1 where SL and SP apical dendrites are, and yet illumination of L1 resulted in stronger SST IPSCs. This could be due to higher density of CheTA in axons compared to somata. The fact that SST exhibits similar target specificity while PV output exhibits opposite target specificity rules out technical bias for illumination. Moreover, NO did not alter output properties of SST neurons, in stark contrast with the enhanced output of L3 PV neurons. Of note, using the same patterned, optical stimulation of L1 versus L3, we reveal opposite connection motifs for PV and SST circuits: this suggests that light was restricted to that particular layer and there was little, if any, spillover to the neighbor layer. The strength of PV output was much stronger than that of SST no matter whether we stimulated the whole field or specific layers (Figure 3), although we cannot rule out some effect of space clamp for SST (dendritic synapses) that made us slightly underestimate its output strength compared to PV (perisomatic synapses). Taken together, this strongly suggests a specific increase in perisomatic (PV) but not dendritic (SST) inhibition following activity deprivation. This is significant as perisomatic inhibition is very potent in controlling excitability and gain control of target neurons.[36] As inhibition shifts from the dendrites to somata during a burst of neural activity,[37] a prediction would be that SL cells are inhibited in the beginning, while SP cells are inhibited in the later, phase of a burst. We believe that the circuit motif and plasticity we uncovered are important for selective gating of principal neuron activity.

4.2 | Experience-dependent plasticity of SP cells

What is the potential physiological consequence of heightened inhibitory plasticity in SP cells? SP cells are preferentially activated by the associational rather than direct OB pathway.[13,14] The associational pathway exhibits life-long synaptic plasticity of excitation,[5] and this could be important for odor-concentration-invariant computation.[3] As SP, but not SL, cells receive recurrent excitation,[13] it is possible that SP cells are better suited for representing learned information whereas SL cells are better suited for representing basic information of odorants (such as identity). One possibility is that excitatory inputs on SP cells are highly plastic, and inhibitory inputs need to match or compensate to maintain a certain level of excitability.[38] Moreover, SP, but not SL, cells extend feedback projections to the OB.[17] An implication is that a modulation of SP cell excitability will change the way OB responds to odorants, while leaving that of SL cells activity intact.[18,19] To our knowledge, our study represents the first report demonstrating a specific plasticity in one of the principal neuron types in APC. Olfactory learning has been shown to modulate synaptic, GABAergic inhibition in the APC.[39] It would be important to investigate whether olfactory learning specifically alters SP inhibition and what the functional consequences are.

Emerging studies show that interneuron to principal neuron connectivity can be target-specific. PV^+, fast-spiking basket cells differentially regulated hippocampal CA1 neurons in that they invoke stronger inhibition to the deep neurons compared to the superficial ones.[40] In the APC, the overall inhibition strength received by L2 principal neurons is higher when L3 is activated compared to L1, but PV versus SST inhibition was not compared.[21,34] These studies consolidate the notion that interneuron subtypes obey specific rules that drive specific target-specific

connectivity. Our study extends on these by demonstrating different connectivity rules for PV and SST output to principal neurons in APC.

4.3 | A model for inhibitory gating of piriform cortical output

Taken together, we propose a new circuit model where (1) PV neurons regulate SL versus SP cells in an opposite manner, with selective, experience-dependent plasticity in the PV → SP microcircuit; and (2) SST neurons regulate SL and SP in a similar fashion (showing laminar but not target specificity; Figure 8). A physiological consequence of this target-specific connectivity is that activation of L1 PV neurons can preferentially suppress SL activity, while activation of L3 PV neurons can preferentially suppress SP activity, gating the output of APC. Based on our findings, we believe that any computational modeling of APC function requires the inclusion of a target- and laminar-specific function of GABAergic inhibition.

ACKNOWLEDGMENTS

This work was supported by the Hong Kong Research Grants Council (RGC/ECS 27103715 to CSWL, RGC/GRF 17128816 to CSWL, RGC/ECS 21103818 to CGL, RGC/GRF 11104320 to CGL, and RGC/GRF 11104521 to CGL), National Natural Science Foundation of China (NSFC/General Program 31571031 to CSWL), Shenzhen General Basic Research Program (JCYJ20190808182203591 to CGL), the Hong Kong Health and Medical Research Fund (HMRF 03143096 to CSWL) and internal funds from City University of Hong Kong (to CGL).

DISCLOSURES

The authors declare no competing financial interests.

AUTHOR CONTRIBUTIONS

He-Hai Jiang performed most of the electrophysiology experiments, some of the naris occlusion, immunofluorescent staining, injections, and analyzed data. Anni Guo performed the LFP recording (Figure 2A–D), immunofluorescent staining, naris occlusion and injections, and analyzed data. Arthur Chiu and Huanhuan Li performed immunofluorescent staining, naris occlusion and injections. Cora Sau Wan Lai contributed to additional reagent. He-Hai Jiang and Chunyue Geoffrey Lau designed the research and wrote the manuscript. All authors contributed to the editing of the manuscript.

CODE AVAILABILITY

All code that supports the findings of this study is available from the corresponding author upon reasonable request.

DATA AVAILABILITY STATEMENT

The data that support the findings of this study are available from the corresponding author upon reasonable request.

ORCID

He-Hai Jiang https://orcid.org/0000-0002-5472-6312
Anni Guo https://orcid.org/0000-0002-1527-3007
Huanhuan Li https://orcid.org/0000-0001-5260-6993
Cora Sau Wan Lai https://orcid.org/0000-0002-5721-4259
Chunyue Geoffrey Lau https://orcid.org/0000-0001-9750-2514

REFERENCES

1. Wilson DA, Sullivan RM. Cortical processing of odor objects. *Neuron*. 2011;72:506-519.
2. Roland B, Deneux T, Franks KM, Bathellier B, Fleischmann A. Odor identity coding by distributed ensembles of neurons in the mouse olfactory cortex. *eLife*. 2017;6:e26337.
3. Bolding KA, Franks KM. Recurrent cortical circuits implement concentration-invariant odor coding. *Science*. 2018;361(6407):eaat6904.
4. Penker S, Licht T, Hofer KT, Rokni D. Mixture coding and segmentation in the anterior piriform cortex. *Front Syst Neurosci*. 2020;14:604718.
5. Poo C, Isaacson JS. An early critical period for long-term plasticity and structural modification of sensory synapses in olfactory cortex. *J Neurosci*. 2007;27:7553-7558.
6. Franks KM, Russo MJ, Sosulski DL, Mulligan AA, Siegelbaum SA, Axel R. Recurrent circuitry dynamically shapes the activation of piriform cortex. *Neuron*. 2011;72:49-56.
7. Choi GB, Stettler DD, Kallman BR, Bhaskar ST, Fleischmann A, Axel R. Driving opposing behaviors with ensembles of piriform neurons. *Cell*. 2011;146:1004-1015.
8. Jung MW, Larson J, Lynch G. Long-term potentiation of monosynaptic EPSPs in rat piriform cortex in vitro. *Synapse*. 1990;6:279-283.
9. Kanter ED, Haberly LB. NMDA-dependent induction of long-term potentiation in afferent and association fiber systems of piriform cortex in vitro. *Brain Res*. 1990;525:175-179.
10. Haberly LB. Parallel-distributed processing in olfactory cortex: new insights from morphological and physiological analysis of neuronal circuitry. *Chem Senses*. 2001;26:551-576.
11. Best AR, Wilson DA. A postnatal sensitive period for plasticity of cortical afferents but not cortical association fibers in rat piriform cortex. *Brain Res*. 2003;961:81-87.
12. Meissner-Bernard C, Dembitskaya Y, Venance L, Fleischmann A. Encoding of odor fear memories in the mouse olfactory cortex. *Curr Biol*. 2019;29:367-380.e4.
13. Suzuki N, Bekkers JM. Two layers of synaptic processing by principal neurons in piriform cortex. *J Neurosci*. 2011;31:2156-2166.
14. Wiegand HF, Beed P, Bendels MHK, Leibold C, Schmitz D, Johenning FW. Complementary sensory and associative microcircuitry in primary olfactory cortex. *J Neurosci*. 2011;31:12149-12158.
15. Diodato A, Ruinart de Brimont M, Yim YS, et al. Molecular signatures of neural connectivity in the olfactory cortex. *Nat Commun*. 2016;7:12238.

16. Padmanabhan K, Osakada F, Tarabrina A, et al. Diverse representations of olfactory information in centrifugal feedback projections. *J Neurosci*. 2016;36:7535-7545.
17. Mazo C, Grimaud J, Shima Y, Murthy VN, Lau CG. Distinct projection patterns of different classes of layer 2 principal neurons in the olfactory cortex. *Sci Rep*. 2017;7:8282.
18. Boyd AM, Sturgill JF, Poo C, Isaacson JS. Cortical feedback control of olfactory bulb circuits. *Neuron*. 2012;76:1161-1174.
19. Otazu GH, Chae H, Davis MB, Albeanu DF. Cortical feedback decorrelates olfactory bulb output in awake mice. *Neuron*. 2015;86:1461-1477.
20. Yang J, Litscher G, Sun Z, et al. Quantitative analysis of axon collaterals of single pyramidal cells of the anterior piriform cortex of the guinea pig. *BMC Neurosci*. 2017;18:25.
21. Large AM, Vogler NW, Mielo S, Oswald A-MM. Balanced feedforward inhibition and dominant recurrent inhibition in olfactory cortex. *Proc Natl Acad Sci U S A*. 2016;113:2276-2281.
22. Tantirigama MLS, Huang HH-Y, Bekkers JM. Spontaneous activity in the piriform cortex extends the dynamic range of cortical odor coding. *Proc Natl Acad Sci U S A*. 2017;114:2407-2412.
23. Hippenmeyer S, Vrieseling E, Sigrist M, et al. A developmental switch in the response of DRG neurons to ETS transcription factor signaling. *PLoS Biol*. 2005;3:e159.
24. Luna VM, Pettit DL. Asymmetric rostro-caudal inhibition in the primary olfactory cortex. *Nat Neurosci*. 2010;13:533-535.
25. Sugai T, Miyazawa T, Fukuda M, Yoshimura H, Onoda N. Odor-concentration coding in the guinea-pig piriform cortex. *Neuroscience*. 2005;130:769-781.
26. Jonas P, Sakmann B. Glutamate receptor channels in isolated patches from CA1 and CA3 pyramidal cells of rat hippocampal slices. *J Physiol*. 1992;455:143-171.
27. Tan AYY, Zhang LI, Merzenich MM, Schreiner CE. Tone-evoked excitatory and inhibitory synaptic conductances of primary auditory cortex neurons. *J Neurophysiol*. 2004;92:630-643.
28. Choy JMC, Suzuki N, Shima Y, Budisantoso T, Nelson SB, Bekkers JM. Optogenetic mapping of intracortical circuits originating from semilunar cells in the piriform cortex. *Cereb Cortex*. 2017;27:589-601.
29. Suzuki N, Bekkers JM. Distinctive classes of GABAergic interneurons provide layer-specific phasic inhibition in the anterior piriform cortex. *Cereb Cortex*. 2010;20:2971-2984.
30. Hu H, Gan J, Jonas P. Interneurons. Fast-spiking, parvalbumin^{+} GABAergic interneurons: from cellular design to microcircuit function. *Science*. 2014;345:1255263.
31. Gunaydin LA, Yizhar O, Berndt A, Sohal VS, Deisseroth K, Hegemann P. Ultrafast optogenetic control. *Nat Neurosci*. 2010;13:387-392.
32. Suzuki N, Bekkers JM. Inhibitory neurons in the anterior piriform cortex of the mouse: classification using molecular markers. *J Comp Neurol*. 2010;518:1670-1687.
33. Large AM, Kunz NA, Mielo SL, Oswald A-MM. Inhibition by somatostatin interneurons in olfactory cortex. *Front Neural Circuits*. 2016;10:62.
34. Large AM, Vogler NW, Canto-Bustos M, Friason FK, Schick P, Oswald A-MM. Differential inhibition of pyramidal cells and inhibitory interneurons along the rostrocaudal axis of anterior piriform cortex. *Proc Natl Acad Sci U S A*. 2018;115:E8067-E8076.
35. Cohen Y, Wilson DA, Barkai E. Differential modifications of synaptic weights during odor rule learning: dynamics of interaction between the piriform cortex with lower and higher brain areas. *Cereb Cortex*. 2015;25:180-191.
36. Freund TF, Katona I. Perisomatic inhibition. *Neuron*. 2007;56:33-42.
37. Stokes CCA, Isaacson JS. From dendrite to soma: dynamic routing of inhibition by complementary interneuron microcircuits in olfactory cortex. *Neuron*. 2010;67:452-465.
38. Froemke RC. Plasticity of cortical excitatory-inhibitory balance. *Annu Rev Neurosci*. 2015;38:195-219.
39. Reuveni I, Lin L, Barkai E. Complex-learning induced modifications in synaptic inhibition: mechanisms and functional significance. *Neuroscience*. 2018;381:105-114.
40. Lee S-H, Marchionni I, Bezaire M, et al. Parvalbumin-positive basket cells differentiate among hippocampal pyramidal cells. *Neuron*. 2014;82:1129-1144.

How to cite this article: Jiang H-H, Guo A, Chiu A, Li H, Lai CSW, Lau CG. Target-specific control of piriform cortical output via distinct inhibitory circuits. *FASEB J*. 2021;35:e21944. doi:10.1096/fj.202100757R